As originally published in the IPC APEX EXPO Conference Proceedings.

Influence of Microstructure on Mechanical Behavior of Bi-Containing Pb-Free Solders

David B. Witkin
The Aerospace Corporation
El Segundo, California

Abstract

SAC-Bi and Sn-Ag-Bi alloys have demonstrated superior performance in thermal cycling reliability tests of printed circuit boards, such as the National Center for Manufacturing Sciences programs in the 1990's and the JCAA-JGPP program of the early 2000's. They have not been widely used in electronics manufacturing despite these promising results due to their Bi content, which has raised concerns for the potential of forming the low-melting point Sn-Pb-Bi eutectic phase (T_m 96 °C) in mixed SnPb-Pb-free soldering. The recently concluded (December 2011) NASA-DoD program Phase II follow-on to JCAA-JGPP revived the possible use of Bi-containing alloys with the recommendation that lower reflow temperatures for ternary Sn-Ag-Bi and quaternary SAC-Bi could reduce potential for pad cratering. At the same time, an explanation for the observed performance in thermal cycling has not been provided, and basic aspects of the metallurgy of these alloys have not been explored to the same extent as more common SAC alloys. In this study, the relationship between microstructure, aging and mechanical behavior was studied for Sn-3.4Ag-4.8Bi and Sn-3.4Ag-1.0Cu-3.3Bi and compared to SAC305. The alloys were prepared in bulk form by rapidly quenching from 260°C resulting in an as-solidified microstructure similar to that observed in solder joints. As-solidified properties were compared to those for samples aged two weeks at 150°C. Tensile testing, constant-stress creep tests, and low-frequency dynamic mechanical analysis up to 50 Hz were performed at various temperatures for both microstructural conditions. Aging led to significant microstructural changes in all the alloys, but while aging was accompanied by changes in the tensile and power-law creep properties of SAC305, the corresponding differences in the as-solidified and aged Bi-containing alloys were either smaller or absent. For example, aging SAC305 led to an increase in the creep stress exponent and a nearly 50% reduction in the activation energy, while for SAC-Bi the reduction in activation energy was similar but the stress exponent was reduced, and in Sn-3.4Ag-4.8Bi neither activation nor stress exponent were changed by aging. These differences do not explain the performance of the solder joints in reliability testing but suggest that thermal fatigue reliability of solder alloys may be enhanced by addition of Bi.

Introduction

SAC-Bi and Sn-Ag-Bi alloys have demonstrated superior performance in thermal cycling reliability tests of printed circuit boards, such as the National Center for Manufacturing Sciences (NCMS) programs in the 1990's [1, 2] and the JCAA-JGPP program of the early 2000's [3]. They have not been widely used in electronics manufacturing despite these promising results due to their Bi content, which has raised concerns for the potential of forming the low-melting point Sn-Pb-Bi eutectic phase (T_m 96 °C) in mixed SnPb/Pb-free soldering. The recently concluded (December 2011) NASA-DoD program Phase II follow-on to JCAA-JGPP revived the possible use of Bi-containing alloys with the recommendation that lower reflow temperatures for ternary Sn-Ag-Bi and quaternary SAC-Bi could reduce potential for pad cratering, as well as possess greater resistance to the growth of tin whiskers [4].

At the same time, an explanation for the performance of Bi-containing alloys documented in thermal cycling has not been provided, and basic aspects of the metallurgy of these alloys have not been explored to the same extent as more common SAC alloys. The original NCMS project on Pb-free solder [1] elected not to pursue this type of characterization of the alloys on the presumption that mechanical properties data for the solders did not necessarily correlate with or provide insight into the reliability of the circuit board, which was the project's motivation. In the present work, the relationship between microstructure, aging and mechanical behavior was studied for Sn-3.4Ag-4.8Bi (SnAg-Bi) and Sn-3.4Ag-1.0Cu-3.3Bi (SAC-Bi) and compared to SAC305. Tensile properties, creep behavior and damping capacity of these alloys were evaluated. The results show significant differences in these properties between the as-cast and aged conditions. In particular, the properties of SAC305 respond to aging differently from the Bi-containing alloys. For example, while aging at 150 °C for 336 hours (2 weeks) decreases the yield and tensile strength of SAC305 by nearly a factor of two, the same aging treatment leads to a much smaller relative change in the strength of SAC-Bi. The relationship between aging, microstructure and mechanical properties do not necessarily explain performance in board-level thermal cycling tests but the metallurgical differences observed between the alloys due to Bi addition could contribute to fundamental basis for improved reliability.

Experimental

Alloy Selection

The alloys that were selected for this study had shown good performance in circuit board reliability testing but had not been extensively characterized and had not been adopted for use by the consumer electronics industry for Pb-free assembly. The alloy selection strategy was based on three suppositions. First, the selection criteria for Pb-free solders in consumer electronics assembly would emphasize cost considerations and regulatory compliance deadlines in product design and manufacturing. Second, the reliability and product lifetime expectations for Pb-free consumer products are entirely different from high-reliability systems, especially space flight hardware where repair and replacement on orbit are not possible. Consequently, the performance and reliability requirements for industries whose products were initially exempt from RoHS would not be considered in alloy selection and development of best assembly practices. The third supposition in alloy selection was that the consumer electronics industry would extensively characterize the Pb-free solder alloys for their systems. Therefore, alloys chosen for this study were those which had shown early promise in circuit-board reliability testing but were subsequently abandoned by the electronics assembly business.

The main sources used for the selection process were the two published by the National Center for Manufacturing Sciences (NCMS) [1, 2, 5] and the US Department of Defense-sponsored Joint Group on Pollution Prevention-Joint Committee on Aging Aircraft (JGPP-JCAA) [3]. Two Bi-containing alloys were selected based on review of these sources:

1. Sn-3.4Ag-4.8Bi (wt. %): This alloy performed well in studies reported by NCMS in 1997 [1], and was the best performer in the initial screening in the 2001 NCMS report [2]. It was dropped from consideration at this point because of its high Bi content. Bi forms a low melting ternary eutectic with Sn and Pb (melting point 96 °C), so this alloy was potentially problematic in a mixed-alloy environment. The actual composition of the alloy reflects the largest amount of Bi that could be added to the Sn-Ag eutectic without showing evidence of Sn-Bi eutectic (melting point 138 °C) during thermal analysis [6].
2. Sn-3.3Ag-1.0Cu-3.4Bi: This alloy was the highly rated in the NCMS 2001 study and was one of the alloys selected for extensive characterization in the JCAA-JGPP study [3]. The alloy outperformed SAC and SnPb in manufactured circuit boards (high Tg board materials) in the latter effort, but did not do as well in reworked boards, in which hand soldering of eutectic SnPb was used to simulate repair of low-temperature circuit boards that had been originally soldered with Pb-free alloys. This specific parameter was intended to duplicate actual practices for aircraft circuit board repair, and it is not certain whether the results for this alloy in these test articles are due to the low-melting Sn-Pb-Bi eutectic or other factors. Subsequent analysis of the test results [7] showed that test alloys were a less important factor in reliability testing than component type for both thermal and vibration testing.

Sample Preparation and Testing

Solder alloys were purchased as bars in pre-alloyed form from commercial vendors. In addition to the two Bi-containing alloys, SAC305 was included as a reference alloy, as were SnPb and commercially pure Sn for selected testing. Specimens for various tests were prepared in bulk form in graphite molds by heating to 270°C and holding for 20 minutes, followed by rapid quenching to room temperature or 0 °C, resulting in as-solidified microstructures similar to that observed in actual solder joints. Samples were tested in as-cast condition or aged condition, which consisted of 336 hours in an inert environment at 150 °C. After casting or aging, specimens were stored in a freezer at -10 °C except during machining or testing.

Tensile specimens were machined from cylindrical blanks as round dogbones with threaded grips to conform to requirements in ASTM E8 standard for tensile testing of metallic materials. The cylindrical castings had a diameter of 9.5 mm, and the tensile specimens were machined with a gauge diameter of 4.1 mm and a gauge length of 16.3 mm. Tensile tests were performed on an Instron (Instron Corp., Norwood Mass.) 8800 series test frame at a strain rate of $8.3 \cdot 10^{-4}$ sec^{-1} at temperatures of 24, 75 and 125 °C. Three or four specimens were run at each temperature for both as-cast and aged conditions of each alloy. Testing conditions were ambient air and samples were allowed to equilibrate for 15-20 minutes prior to beginning the test. Strain measurements were made using a video extensometer.

Creep specimens were of a double shear geometry inspired by earlier work on the creep of pure Sn and pure Pb [8]. The specimen features three grip sections of identical diameter and two reduced gauge sections. The specimen is held at each end and pulled in the middle by a fixed load, and approximates a constant stress condition to high strains. Specimens were machined from cylindrical castings with a diameter of 12.5 mm to dimensions of approximately 23 mm in length and an overall diameter of 11.5 mm. The reduced gauge sections were each 2 mm long and 5.7 mm diameter. The specimen geometry is intended to keep the specimen at constant shear stress during the test, although pure shear is not strictly attained. Tests were performed at 42, 75, 100 and 125 °C by submersing the sample and fixturing into a heating silicone oil bath. Room temperature tests were performed under ambient laboratory conditions. Temperature fluctuations in both cases were

less than ±1 K over the duration of the tests. Creep tests were performed at ranges in applied stress equivalent to approximately 20 to 90 percent of the yield strength in tension, which worked out to a range of applied shear stress from 3.5 MPa to 60 MPa, depending on the alloy and condition. The higher-strength Bi-containing alloys required higher creep test stresses and accounted for the higher test loads.

Displacement of the samples was measured with an accuracy of 5×10^{-4} mm, or a strain of approximately 9×10^{-5}. Tests were concluded no sooner than having met one of two conditions: a) rupture or clear evidence of the onset of tertiary creep, or b) extended period of apparent steady-state creep through a minimum test duration of 2.5×10^{5} seconds (approximately 3 days). Several tests were run in excess of 5×10^{5} seconds. The nature of the alloys was that true steady-state secondary creep was not attained so a minimum creep rate was substituted for steady-state creep rate where necessary.

Specimens for dynamic mechanical analysis (DMA) were prepared from rectangular graphite molds that yielded bars measuring approximately 60 x 6.4 x 3.2 mm. These rectangular bars were reduced to a thickness of approximately 1.7 mm by manually grinding and lapping roughly equal amounts of material from each face. DMA was performed using a TA Instruments Q800 DMA in dual cantilever mode, in which the rectangular beam sample was fixed at its ends and the middle. Tests were run in both isothermal and temperature sweeping modes. For the former, measurements at frequencies from 0.1 to 200 Hz were collected at 0 and 24 °C and displacements of 5, 10 and 20 μm. A complete set of alloys and aging conditions were run in duplicate only at 5 μm, which for a nominal beam thickness of 1.7 mm was equivalent to a strain of approximately $7.5 \cdot 10^{-5}$. Measurements above 50 Hz were discarded due to instrumental factors. Comparison of alloys in isothermal mode is made here most extensively for tests run at 0 °C because at the lower temperature there was less dependence of measured tan δ on strain. Additional tests were run as temperature sweeps using a displacement of 5 μm at fixed frequencies from temperatures of -100 to +100 °C.

Results

Microstructures

Details of as-cast and aged microstructures, including micrographs, of SAC-Bi, SnAg-Bi and SAC305 for the tests discussed herein have been previously published [9, 10] and are only summarized here. As reference, previously unpublished metallographic images of SAC305 at 400X magnification are provided in Figure 1, and SAC-Bi and SnAg-Bi in **Figure 2**. All three alloys share similarities in their microstructures and response to aging. In the as-cast condition the microstructure is dominated by the dendritic structure exemplified in Figure 1. Individual intermetallic particles that formed upon solidification ($SnAg_3$ and Sn_5Cu_6) were too small to be resolved even at 10,000X magnification in a scanning electron microscope. Aging at 150 °C for 336 hours leads to ripening of these particles and loss of dendritic structure. Intermetallic particles are typically found stabilizing irregular grain boundaries.

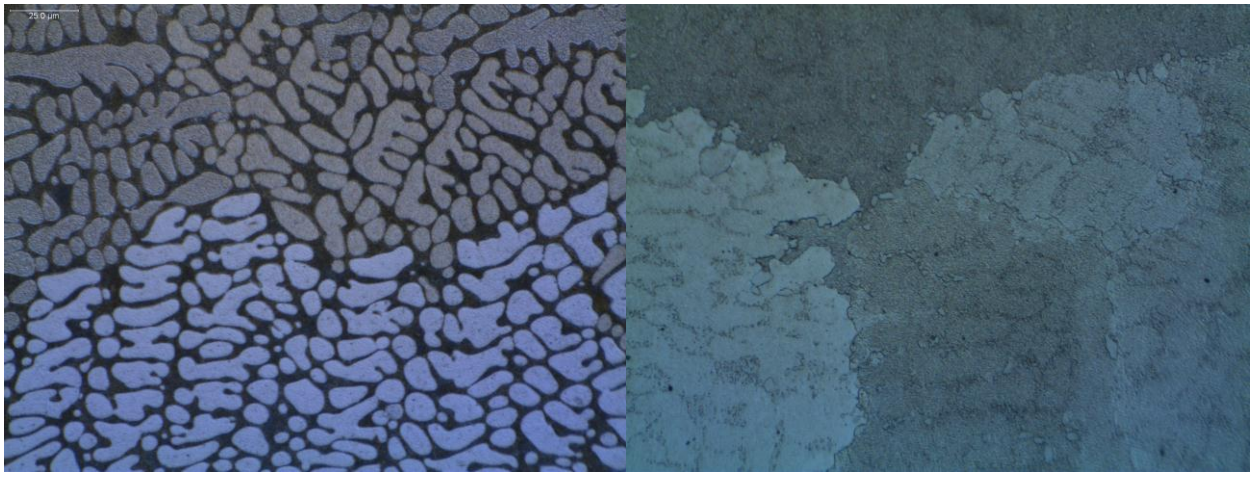

Figure 1. Optical micrographs of as-cast (left) and aged (right) SAC305

The story for the two Bi-containing alloys is similar with respect to grain boundaries and Sn-Ag and Sn-Cu compounds. Bi does not form compounds with Sn, Cu or Ag, so it is present either in solid solution or as a separate elemental phase. In as-cast SAC-Bi, Bi particles solidify at the edges of individual Sn dendrites. Given the undercooling of the primary β-Sn phase that occurs during solidification of Pb-free solders and the relatively low temperature of the binary Sn-Bi eutectic, the location of Bi particles is interpreted as evidence that the boundary between primary tin dendrites and eutectic regions is the last part of the melt to solidify. After aging, Bi precipitates are found predominantly found at grain boundaries. The solubility

of Bi in Sn at the 423 K aging temperature exceeds the Bi content of the alloy, so the preferential nucleation and growth of Bi at heterogeneous nucleation sites due to aging suggests either that the Bi diffused rapidly at room temperature after aging or was retained at grain boundaries even during extended aging.

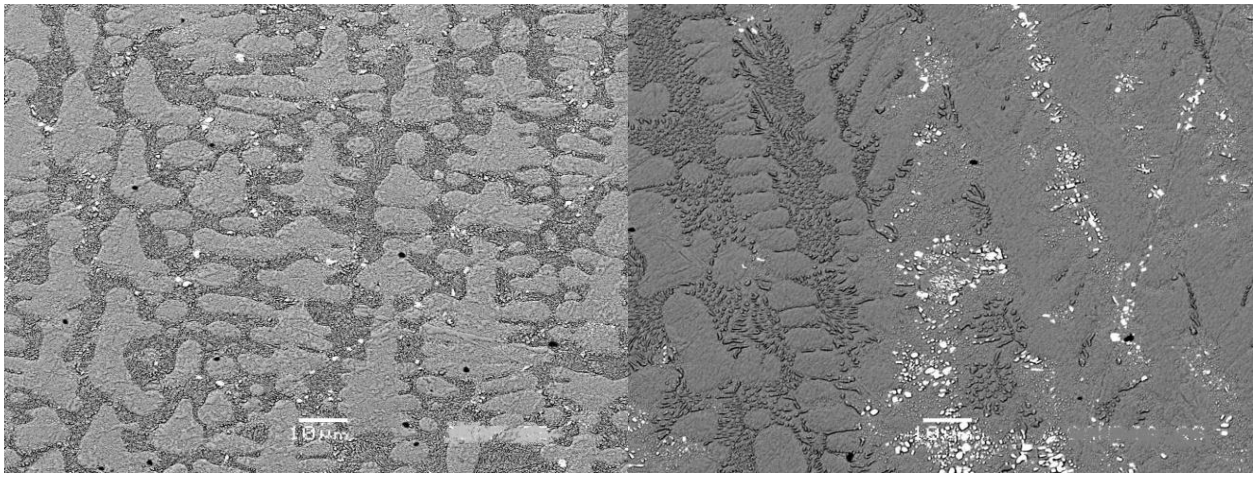

Figure 2. SEM BSE micrographs (1000X) of as-cast microstructure of SAC-Bi (left) and SnAg-Bi (right)

The trends observed in SAC-3.4Bi are also true for SnAg-4.8Bi, but the distribution of Bi through the alloy is different due to differing Bi content. In the as-cast SnAg-Bi the Bi particles are found in the interior of the Sn dendrites (Figure 2), not at the dendrite-eutectic interface as in SAC-Bi. The logic for the SAC-Bi leads to the conclusion that the solidification of the Sn phase proceeds from the eutectic region to the interior of the dendrites. After aging the Bi distribution consists of 1 to 5 μm equiaxed particles along grain boundaries and a fine dispersion of sub-micrometer particles throughout grain interiors. The room-temperature solubility of Bi in Sn is approximately 1.8 wt %, so the SnAg-Bi alloy contains approximately twice the Bi beyond the solubility limit as the SAC-Bi alloy. This difference accounts for the different microstructures in the aged condition of the two alloys.

The anisotropy of the tetragonal β-Sn unit cell has been noted for its influence on both mechanical behavior of Pb-free solder [11] and solder joint reliability [12]. The crystallographic orientation of various samples was not assessed in the current work but there is no indication that results were unduly influenced by preferred orientation or very large grain sizes. The influence of preferred orientation of the Sn unit cell with respect to applied loads in the various tests should thus be considered part of the systematic error in the reported results.

Tensile Properties

Tensile properties (yield strength and ultimate tensile strength) for tensile tests performed at three temperatures are summarized in Table 1. The Castin™ (AIM Solder) alloy was also tested and is included in the table. The change in yield or ultimate strength due to aging is shown as a percentage.

Table 1. Tensile Properties of Solders (all values in MPa; average of three or four specimens per condition)

	SAC305						SAC-Bi					
	Yield			UTS			Yield			UTS		
Test Temperature (°C)	As Cast	Aged	Change (%)	As Cast	Aged	Change (%)	As Cast	Aged	Change (%)	As Cast	Aged	Change (%)
25	39.0	23.0	-41.1	43.1	27.0	-37.4	65.4	57.1	-12.7	79.5	78.2	-1.6
75	31.4	14.2	-54.8	33.1	15.5	-53.2	57.1	46.9	-17.8	60.7	52.1	-14.1
125	24.1	13.9	-42.6	24.6	14.3	-41.7	39.3	35.6	-9.5	40.4	37.0	-8.3
	SnAg-Bi						Sn-2.5Ag-0.8Cu-0.5Sb (Castin)					
	Yield			UTS			Yield			UTS		
	As Cast	Aged	Change (%)	As Cast	Aged	Change (%)	As Cast	Aged	Change (%)	As Cast	Aged	Change (%)
25	58.3	55.4	-4.9	81.4	83.6	2.7	39.8	26.3	-33.9	45.3	30.5	-32.8
75	46.1	46.3	0.3	53.1	57.8	8.7	30.9	19.2	-38.0	33.5	20.2	-39.8
125	38.4	38.2	-0.5	40.6	39.8	-1.8	20.4	14.0	-31.6	21.8	14.6	-32.9

There are two primary trends in Table 1. The first is the large difference in strength imparted to the SAC-Bi and SnAg-Bi alloys by the addition of Bi, and the second is the differences among the alloys in response of strength to aging. In SAC305, the considerable drop off in strength after aging is attributed to the loss of intact eutectic regions which constrain the deformation of the relatively softer primary β-Sn. The aged microstructure contains relatively less abundant and much larger intermetallic particles that are primarily found at grain boundaries. In uniaxial tension it is expected that these grain boundary particles do not strengthen SAC305 and the drop in strength due to aging is dramatic, a result consistent with other investigations [13, 14].

The influence of Bi on Pb-free solder mechanical properties have been attributed to a combination of solid solution and particle strengthening for both SAC-Bi and SnAg-Bi [9]. The results in Table 1 show that the while the strengths of SAC-Bi and SnAg-Bi respectively are not too different from each other in the as-cast condition, the alloys respond to aging differently. The strength of SAC-Bi decreases after aging, although less in absolute and much less in relative terms than was observed for SAC305. In contrast, the strength of SnAg-Bi remains nearly constant. The microstructural changes that occur in aging of SAC-Bi are similar to those observed in SAC305, with the additional feature of precipitation of grain boundary Bi particles. Therefore, the strength is diminished in a similar way by the loss of particle-reinforced eutectic regions, an effect which is countered by the presence of Bi in solid solution. Aging of SnAg-Bi leads to a ripening of Ag_3Sn particles and erosion of the eutectic region but it is accompanied by a redistribution of Bi particles that results in a fine dispersion of Bi throughout grain interiors, not only at grain boundaries. The small changes in tensile properties for this alloy are somewhat surprising in light of the dramatic differences between the as-cast and aged microstructure. This too is understood as the dual contribution to strengthening by Bi as particles and in solid solution, although the relative contributions of the two types of strengthening cannot be determined based on this data.

Creep

Creep data for Pb-free solder alloys and multiple sample scales (e.g., bulk, lap shear and solder-joint scale) have been analyzed using both hyperbolic sine models and power law models [15, 16]:

$$\dot{\gamma} = A\sinh^n(B\tau)\exp\left[\frac{-Q}{RT}\right] \qquad \text{Hyperbolic Sine Model}$$

$$\dot{\gamma} = A\frac{G}{T}\left(\frac{\tau}{G}\right)^n \exp\left[\frac{-Q}{RT}\right] \qquad \text{Power Law Model}$$

Creep data were analyzed in detail using both models in a previous publication [10], but it should be noted that in that publication the use of hyperbolic sine model was used to compare the data for SAC-Bi and SnAg-Bi alloys to published data for dilute Sn-Bi alloys [17] and to compare as-cast and aged SAC305 to published data for as-cast [18] and aged [19] bulk SAC396. The hyperbolic sine model may have merit as a modeling tool for solder joint deformation calculations, but when confronted with a change in creep behavior as a function of applied stress, it can obscure the actual operative creep mechanisms by rolling all data into a single expression with one stress exponent and activation energy. For example, comparing creep data for SAC305 at 75 °C reveals key differences between the as-cast and aged condition, as shown in Figure 3:

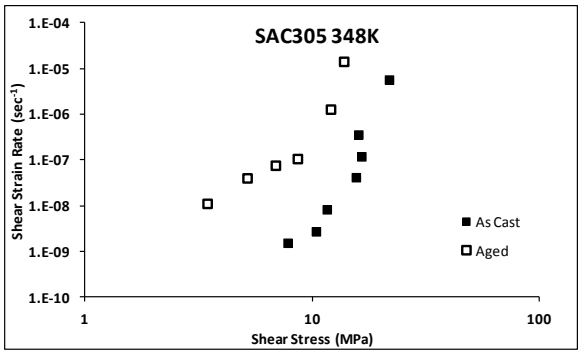

Figure 3. Creep data for as-cast and aged SAC305 tested at 75 °C

The as-cast SAC305 can be fit using a single power-law model, while the aged alloy could be fit using either a single hyperbolic sine function or a combination of a low-stress and high-stress power law function. In the case of aged SAC305,

the change from a lower stress exponent at lower stress (n = 2.5) to a higher stress exponent (n = 7.8) at applied shear stress above roughly 10 MPa at 75 °C may mean that a different deformation mechanism needs to be considered at different loads, and that the transition between the two regimes is not likely to occur at the same shear stress in aged SAC305 as it does in as-cast SAC305. In general for all three alloys the transition between low and high stress occurs at a temperature-compensated shear stress τ/G (where G is shear modulus) of approximately 4×10^{-4}.

While the previous publication provides details of the creep model parameters n and Q for each equation, a rough summary of the observations for all three alloys can be made using a single figure showing the measured steady-state or minimum shear strain rate as a function of temperature under a constant stress of 8.7 MPa, as shown in Figure 4.

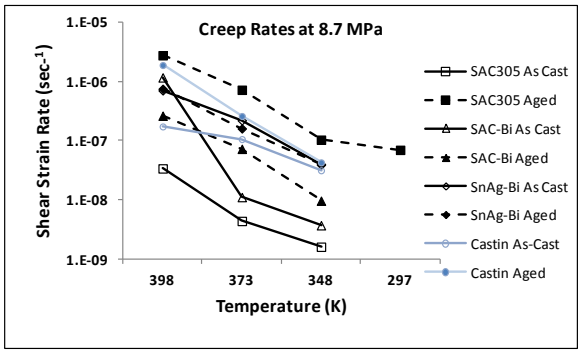

Figure 4. Comparison of shear strain rates of alloys in aged and as-cast condition [10]. Previously unpublished results for Castin (SAC-Sb) are also shown.

While higher applied loads were necessary during testing to complete tests in a reasonable amount of time, lower stresses such as 8.7 MPa (~1250 psi) are more representative of the types of thermomechanical loads that might be expected in solder joints in actual applications. In this case, the data show that SAC305 is most creep resistant in the as-cast condition, but in the aged condition it deforms more rapidly than any other alloy. The 8.7 MPa stress in Figure 4 is a larger fraction of the yield strength in as-cast SAC305 than for SAC-Bi or SnAg-Bi, so the change in creep strain rates in SAC305 with aging is due to the shift to the high stress regime with higher stress exponent n for the aged alloy even though at the same applied load. At the other extreme, the measured creep strain rates for SnAg-Bi do not change due to aging.

While the details of creep analysis are important, the quantitative results of creep testing can be summarized as follows [10]:

- Aging decreases the apparent activation energy of creep for SAC305 and SAC-Bi;
- Aging has minimal effect on the activation energy of SnAg-Bi; and
- The activation energy of creep in SAC305 is lower than SAC-Bi and SnAg-Bi in either as-cast or aged conditions.

In practical terms, the implications of the first two of these three statements are captured to a great extent in Figure 4: the creep rates of SAC305 and SAC-Bi will change with the microstructural changes that occur during aging, but the creep rate of SnAg-Bi will remain nearly constant. It has been found that extended aging of SnPb at 125 °C had minimal effect on room-temperature creep rates of Sn-37Pb [13], so the behavior of SnAg-Bi is similar to SnPb in that respect.

Damping Capacity

Damping capacity is reported as loss tangent (tanδ), where the loss angle δ represents the phase angle between stress and strain. The loss angle is related to the engineering quantity specific damping capacity Ψ by the relationship:

$$\Psi = 2\pi \tan\delta$$

The specific damping capacity refers to the ratio of the energy dissipated to maximum elastic energy stored [20]; in the DMA testing the source of the elastic energy is the cantilever bending imposed by the test frame. Presumably higher damping capacity could lead to better dynamic performance, with less elastic energy from impacts available to cause failures in intermetallics or pad cratering. For SAC solders the energy stored during the input of elastic energy may provide a similar driving force for microstructural evolution as observed during isothermal aging, although by a different route than particle coarsening. For example, decrease in hardness was measured as a function of shear fatigue cycles even though the typical intermetallic particle size did not change as a result of the applied elastic/plastic loads [21].

Comparison of isothermal (at 0 °C) damping data over frequencies from 0.1 to 50 Hz is shown in presentation charts accompanying this manuscript. The testing temperature is sufficiently high relative to the melting points of the alloys that at 0 °C the damping behavior is attributed to thermally activated dislocation movement that is sensitive to microstructural factors such as grain size and dislocation density [22]. Literature data for high purity tin [23] are seen to be consistent with the present data, including the small absorption peak that occurs in several alloys but not Sn-37Pb. The general behavior of all of the Pb-free alloys appears to be consistent with the response of the β-Sn matrix to the elastic input, while the differences between them are attributed to individual characteristics of the microstructures. While the log-log nature of the tanδ vs. frequency plots obscures the magnitude of the change between as-cast and aged Sn-37Pb, there is a roughly 0.011 decrease in tanδ due to aging, which is the largest measured change of all the alloys. The coarsening of lamellae in Sn-37Pb leads to reduction in the number of phase boundaries which is presumably responsible for the decrease in damping. In the Pb-free alloys, the behavior of SAC305 with respect to aging is the opposite of SAC-Bi and SnAg-Bi, as aging SAC305 leads to an increase in damping capacity while it is decreased in the Bi-containing alloys. For SAC305, the positive change is attributed to the formation of a continuous Sn matrix. For SAC-Bi and SnAg-Bi the decrease is consistent with the general notion that a coarsening of the microstructure and annealing reduces damping capacity.

The plot of tanδ vs. temperature at a single frequency (in this case 10 Hz) in the presentation charts shows that considering the data at only 0 °C does not provide a complete picture of the behavior of these alloys. As the test temperature reaches room temperature and above, tanδ of the Bi-containing alloys increases dramatically relative to SAC305, so that above 50 °C damping capacity of SnAg-Bi actually exceeds SAC305 while SAC-Bi exceeds SAC305 in the as-cast condition. The trends in damping capacity as a function of temperature can be compared to results for commercially pure Sn and Sn-37Pb. This comparison shows that SAC305 behaves like Sn, exhibiting a gradual and relatively small change over the 200-degree change from – 100 to + 100 °C. SAC-Bi and SnAg-Bi are more like SnPb, in which a relatively large increase in tanδ occurs as temperature increases past room temperature. Given the similarities between the binary phase diagrams of Sn-Pb and Sn-Bi, the results for damping capacity indicate that the Sn-Bi interfaces are more important in determining the behavior of SAC-Bi and SnAg-Bi than the intermetallic particle-Sn matrix interfaces in SAC305.

Conclusions

The objective of this research was to characterize the mechanical metallurgy of alternative solder alloys for high-reliability applications. Key differences in use of high-reliability electronic systems compared to mass-produced consumer electronic devices include harsh deployment environments and length of service life. Electronic systems installed in a satellite, for example, may be built years before the spacecraft is launched and then must survive many years in orbit with no opportunity for repair or replacement. The system life cycle, sustainability requirements and usage environments for space vehicles differ from airborne systems and there is no reason to expect that the optimal solder alloy for space is the same for aircraft. Characterizing behavior and performance of solder joints over long time scales may not be a high priority for consumer electronics manufacturers, although the documented changes in SAC alloy microstructures due to isothermal aging and their impact on reliability have been documented [24, 25].

The selection of Bi-containing alloys was based on their performance in early circuit-board reliability testing programs. The mechanical behavior of these alloys shows that the addition of Bi to SnAg or SAC leads to a different response to isothermal aging than is seen in SAC305. These results do not necessarily explain the performance of Bi-containing alloys in reliability testing, but they do show the extent to which the mechanical behavior of different alloys can vary. The results of this research demonstrates the need for microstructure-based material properties for modeling of solder joint behavior in long lifetime high-reliability systems but they also suggest that the additions of small amounts of Bi could decrease changes in solder alloy properties over time and result in more readily predictable solder joint deformation.

Acknowledgements

The research described here was supported by The Aerospace Corporation's Independent Research and Development program, and was undertaken with the enthusiastic support of Dr. L. Parker Temple III. I thank numerous colleagues for their contributions: Dhruv Patel, Ben Nelson, Byron Zeigler, Jay Yamasaki, Robert Castaneda, and Brian Gable, as well as student interns Kareem Hammoud, Jonathan Salfity and Swati Bhanderi. All trademarks, service marks and trade names are the property of their respective owners.

References

[1] NCMS, Lead-Free Solder Project: Final Report, National Center for Manufacturing Sciences, Ann Arbor, Mich., 1997.
[2] NCMS, Lead-free, High-temperature, Fatigue-resistant solder: Final Report, National Center for Manufacturing Sciences, Ann Arbor, Mich., 2001.
[3] JCAA-JGPP, JCAA-JGPP Lead Free Solder Project Joint Test Report, Executive Summary, International Trade Bridge, Dayton, Ohio, 2006.

[4] NASA TEERM, NASA-DoD Lead-Free Electronics Project Joiint Test Report, December 2011.
[5] F.W. Gayle, G. Becka, J. Badgett, G. Whitten, T.Y. Pan, A. Grusd, B. Bauer, R. Lathrop, J. Slattery, I. Andersen, J. Foley, A. Gickler, D. Napp, J. Mather, C. Olson, JOM, 53 (2001) 17-21.
[6] P.T. Vianco, J.A. Rejent, J. Elec. Mat., 28 (1999) 1127-1137.
[7] D. Fritz, B. Russell, G. Latta, in: 7th IPC International Conference on Reliability, Rework and Repair of Lead-Free Electronics, IPC, Raleigh, NC, 2008.
[8] F.A. Mohamed, K.L. Murty, J.W. Morris, Met. Trans. A, 4 (1973) 935-940.
[9] D.B. Witkin, Mat. Sci. Eng. A, 532 (2012) 212-220.
[10] D.B. Witkin, J. Elec. Mat., 41 (2012) 190-203.
[11] A.U. Telang, T.R. Bieler, A. Zamiri, F. Pourboghrat, Acta Mat., 55 (2007) 2265-2277.
[12] T.K. Lee, B. Zhou, L. Blair, K.C. Liu, T.R. Bieler, J. Elec. Mat., 39 (2010) 2588-2597.
[13] H. Ma, J.C. Suhling, Y. Zhang, P. Lall, M.P. Bozack, 57th IEEE ECTC (2007), 653-668.
[14] Y. Zhang, Z. Cai, J.C. Suhling, P. Lall, M.P. Bozack, 58th IEEE ECTC (2008), 99-112.
[15] J.-P. Clech, SMTAI04, Proceedings, SMTA (2004).
[16] H. Ma, J. Mat. Sci., 44 (2009) 3841-3851.
[17] D. Mittlin, C.H. Raeder, R.W. Messler, Met. Mat. Trans. A, 30 (1999) 115-122.
[18] P.T. Vianco, J.A. Rejent, A.C. Kilgo, J. Elec. Mat., 33 (2004) 1389-1400.
[19] P.T. Vianco, J.A. Rejent, A.C. Kilgo, J. Elec. Mat., 33 (2004) 1473-1484.
[20] R.S. Lakes, Rev. Sci. Inst., 75 (2004) 797-810.
[21] L. Yang, L. Yin, B. Roggeman, P. Borgesen, 60th IEEE ECTC (2010) 1518-1523.
[22] A.S. Nowick, B.S. Berry, Anelastic Relaxation in Crystalline Solids, Academic Press, New York, 1972.
[23] L.S. Cook, R.S. Lakes, Scripta Met. Mat., 32 (1995) 773-777.
[24] V. Venkatadri, L. Yin, Y. Xing, E. Cotts, K. Srihari, P. Borgesen, 59th IEEE ECTC (2009) 398-405.
[25] T.K. Lee, W. Xie, B. Zhou, T.R. Bieler, K.C. Liu, J. Elec. Mat., 40 (2011) 1967-1976.